

Ali BELHOCINE <sup>1</sup>, Nadica STOJANOVIC<sup>2</sup>,  
Oday Ibraheem ABDULLAH<sup>3</sup>

## Numerical predictions of laminar flow and free convection heat transfer from an isothermal vertical flat plate

Received 26 March 2022, Revised 24 May 2022, Accepted 4 July 2022, Published online 14 November 2022

**Keywords:** free convective flow, vertical flat plate, similarity solution, boundary layer flow, dimensionless temperature, Prandtl number, Runge-Kutta method

In this present work, the laminar free convection boundary layer flow of a two-dimensional fluid over the vertical flat plate with a uniform surface temperature has been numerically investigated in detail by the similarity solution method. The velocity and temperature profiles were considered similar to all values and their variations are as a function of distance from the leading edge measured along with the plate. By taking into account this thermal boundary condition, the system of governing partial differential equations is reduced to a system of non-linear ordinary differential equations. The latter was solved numerically using the Runge-Kutta method of the fourth-order, the solution of which was obtained by using the FORTRAN code on a computer. The numerical analysis resulting from this simulation allows us to derive some prescribed values of various material parameters involved in the problem to which several important results were discussed in depth such as velocity, temperature, and rate of heat transfer. The definitive comparison between the two numerical models showed us an excellent agreement concerning the order of precision of the simulation. Finally, we compared our numerical results with a certain model already treated, which is in the specialized literature.

---

✉ Ali Belhocine, e-mail: [al.belhocine@yahoo.fr](mailto:al.belhocine@yahoo.fr)

<sup>1</sup>Department of Mechanical Engineering, University of Sciences and the Technology of Oran, Algeria. ORCID:0000-0001-7957-7571

<sup>2</sup>University of Kragujevac, Faculty of Engineering, Department for Motor Vehicles and Motors, Serbia

<sup>3</sup>System Technologies and Mechanical Design Methodology, Hamburg University of Technology, Hamburg, Germany



© 2022. The Author(s). This is an open-access article distributed under the terms of the Creative Commons Attribution (CC-BY 4.0, <https://creativecommons.org/licenses/by/4.0/>), which permits use, distribution, and reproduction in any medium, provided that the author and source are cited.

## Nomenclature

$C_p$	specific heat at constant pressure, $\text{J kg}^{-1}\text{K}^{-1}$
$D$	distance, m
$F$	dimensionless stream function
$G$	dimensionless temperature
Gr	Grashof number
$g$	gravitational acceleration, $\text{ms}^{-1}$
$k$	thermal conductivity, $\text{Wm}^{-1}\text{K}^{-1}$
$L$	length, m
$\text{Nu}_x$	local Nusselt number
$p$	pressure, $\text{kg m s}^{-2}$
Pr	Prandtl number
$q$	heat transfer rate per unit area, $\text{Wm}^{-2}$
$T$	temperature, K
$T_1$	fluid temperature, K
$T_w$	wall temperature, K
$U$	dimensionless velocity
$u$	velocity component, $\text{ms}^{-1}$
$u_r$	fluid velocity, $\text{ms}^{-1}$
$V$	dimensionless velocity
$v$	velocity component, $\text{ms}^{-1}$
$x$	distance, m
$x$	coordinate direction, m
$y$	coordinate direction, m

### Greek letters

$\beta$	thermal expansion, $\text{K}^{-1}$
$\delta$	velocity boundary layer thickness, m
$\eta$	similarity variable, m
$\theta$	dimensionless temperature
$\mu$	dynamic viscosity, $\text{kgm}^{-1}\text{s}^{-1}$
$\nu$	kinematic viscosity, $\text{m}^2\text{s}^{-1}$
$\rho$	density, $\text{kgm}^{-3}$
$\phi$	angular coordinate, deg

## 1. Introduction

As has been recognized, free or natural convection is a heat transfer between a surface and a fluid moving over it, in which the motion of the fluid is wholly caused by the presence of the buoyant forces which arise as a result of density changes producing temperature changes in the flow. Free-convection flow is a principal mode of heat-transfer in several engineering applications such as in the fields of nuclear engineering, aeronautics, and gas turbines industry. Boundary layer flows with internal heat generation past a vertical plate continues to receive consider-

able attention because of its many practical applications in a broad spectrum of engineering systems like geothermal reservoirs, cooling of nuclear reactors, thermal insulation, combustion chamber, rocket engine, etc. Many principal previous studies concerning laminar natural convective flows over a vertical flat plate have been found in the literature and these problems may admit similarity solutions. Jashim Uddin et al. [1] have numerically investigated the combined heat and mass transfer by free convective flow along a moving vertical flat plate with thermal convective boundary conditions using similarity solutions. In the work by Esfahani and Bagherian [2], a similarity solution was applied to perform an analysis of unsteady free convection flow over a vertical flat plate immersed in a power law fluid. Boutros et al. [3] performed a numerical analysis of the problem of steady laminar free convection from a nonisothermal vertical flat plate while applying solution transformations. Modather et al. [4] presented an analytical study of MHD heat and mass transfer oscillatory flow of a micropolar fluid over a vertical permeable plate in a porous medium. Veera Krishna and Chamkha [5] investigated the Hall and ion slip effects on the MHD convective flow of elastico-viscous fluid through a porous medium between two rigidly rotating parallel plates. Veera Krishna and Chamkha [6] analyzed the diffusion-thermo, radiation-absorption, and Hall and ion slip effects on MHD free convective rotating flow of nano-fluids past a semi-infinite permeable moving plate. Veera Krishna et al. [7] investigated the Hall and ion slip effects on the unsteady magnetohydrodynamic (MHD) free convective rotating flow over an exponentially accelerated inclined plate through a saturated porous medium. The implicit finite difference method is more accurate and it has been adopted in certain works, like Chamkha [8, 9]. In the works carried out by Rasool et al. [10], Chamkha et al. [11], the problems of flow through a porous medium over a flat surface have been solved numerically on the basis of the method of transformations. Chamkha and Ben-Nakhi [12], Chamkha [13] conducted mathematical modeling of a heat transfer in free and mixed convection over an inclined plate and isothermal vertical surface in a porous medium. Wakif et al. [14] established a numerical solution of the electro-magneto-hydrodynamic convective flow of a viscous electrically conducting fluid over a horizontal Riga plate. Ahammad et al. [15] presented a numerical investigation of heat transfer in a porous medium adjacent to a vertical plate whose problem was solved using the finite difference method. Veera Krishna et al. [16] conducted numerical investigation on the effects of thermal radiation and rotation on the unsteady MHD convective flow past an infinite vertical moving absorbent plate using both similarity transformations and cubic B-splines collocation method. Several authors [17–19] have performed numerical simulations on the phenomenon of natural convection. In the work of Zhou et al. [20], a numerical simulation was carried out to study the unsteady natural convection flow. Talluru et al. [21] conducted an experimental study on a natural convection boundary layer over a hot vertical plate. The same problem of natural convection has been the subject of other numerical investigations [22–26]. Recently, countless analytical and numerical methods have been exploited for

the study of natural convection [27–41]. In the works carried out by Belhocine et al. [42–46], analytical and numerical methods have proven their efficiency in the treatment and resolution of certain thermal problems such as the method of separation of variables, orthogonal collocation, and the Runge-Kutta method of the fourth-order. Ostrach [47] studied the similarity solutions for the laminar free convection flow of a fluid over a vertical flat plate.

The main objective of this work is to present a mathematical formulation of the two-dimensional flow problem of free convection of the laminar boundary layer of a fluid through an isothermal vertical flat plate.

The novelty of the work is to illustrate how similarity solutions have been exploited in solving the free convective flow problem as well as the use of the implicit fourth-order Runge-Kutta method (RK4) with a step size control, integration algorithm to discretize the non-linear PDEs describing the laminar boundary layer flow and as a sequential numerical method of ODEs system. Since we focused on the analysis of the problem in the case of a free convective flow, the properties of the fluid were supposed constant except the density that varies only with the temperature which gives rise to the buoyancy force. The methodology followed here deals with the possibility of the existence of similarity solutions for this flow problem. It has been established that the similarity solution can only be found if the variation in velocity and temperature of the plate is a function of the distance from the leading edge measured along the plate. The partial differential equations together with the thermal boundary condition describing the model were all transferred to a system of non-linear ordinary differential equations which have been considered to be solved by the Runge-Kutta technique of the fourth-order and which were programmed in FORTRAN code. Several important results were derived from the analysis and discussed deeply such as dimensionless temperature, velocity, and rate of heat transfer. At the end of the contribution, we compared our results with those found in the literature. The observation established thanks to this comparison showed us that the two models are in a good agreement, which automatically validates the results of our numerical simulation.

## 2. The characteristic velocity

We have employed for the solution of the problem suitable dimensionless variables to express in terms of the governing equations while introducing the appropriate characteristic velocity.

If the wall temperature is  $T_{wr}$ , then the buoyant force per unit volume in the flow is equal to  $\beta g \rho (T_{wr} - T_1)$ . The work done by the buoyant forces on the fluid per unit volume of fluid is  $\beta g \rho (T_{wr} - T_1) D$ , where  $D$  is the distance from the body.

To derive the expression for velocity, we equalize the kinetic energy from the work done by the buoyancy forces, hence

$$\beta g \rho (T_{wr} - T_1) D = \frac{1}{2} \rho u_r^2. \quad (1)$$

From Eq. (1), we can get

$$u_r = \sqrt{2\beta g (T_{wr} - T_1) D}. \quad (2)$$

Therefore, the characteristic velocity will be taken as:  $u_r = \sqrt{\beta g (T_{wr} - T_1) L}$ .

Here,  $L$  is a reference length that characterizes the size of the surface, e.g., its length.

### 3. Governing equations of fluid flow

For a steady two-dimensional flow in natural convection, the governing equations are defined as:

$$\frac{\partial u}{\partial x} + \frac{\partial v}{\partial y} = 0, \quad (3)$$

$$u \frac{\partial u}{\partial x} + v \frac{\partial u}{\partial y} = -\frac{1}{\rho} \frac{\partial p}{\partial x} + \nu \left( \frac{\partial^2 u}{\partial x^2} + \frac{\partial^2 u}{\partial y^2} \right) + \beta g (T - T_1) \cos \phi, \quad (4)$$

$$u \frac{\partial v}{\partial x} + v \frac{\partial v}{\partial y} = -\frac{1}{\rho} \frac{\partial p}{\partial y} + \nu \left( \frac{\partial^2 v}{\partial x^2} + \frac{\partial^2 v}{\partial y^2} \right) + \beta g (T - T_1) \sin \phi, \quad (5)$$

$$u \frac{\partial T}{\partial x} + v \frac{\partial T}{\partial y} = \left( \frac{k}{\rho c_p} \right) \left( \frac{\partial^2 T}{\partial x^2} + \frac{\partial^2 T}{\partial y^2} \right), \quad (6)$$

where  $T_1$  is the undisturbed temperature away from the surface. Due to the existence of low velocities, dissipation is neglected in the energy equation (6).

The energy equation (6) and the continuity equation (3) are similar to those for forced convective flow. Given the presence of buoyancy terms, the momentum equations (4) and (5) are practically distinct from those of forced convective flows. The angle in these buoyancy terms between the  $x$ -axis and the vertical is defined by  $\phi$  as shown in Fig. 1.

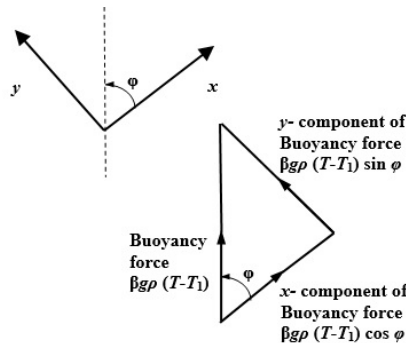


Fig. 1. Definition of the components of Buoyancy force

## 4. Similarity solutions for free convective laminar boundary layer flows

### 4.1. Problem description

In the case of free convective flows and in order to explain the similarity solution procedure, we initially considered a vertical flat plate subjected to a two-dimensional flow and with a uniform surface temperature. The following Fig. 2 illustrates the situation of the physical model considered.

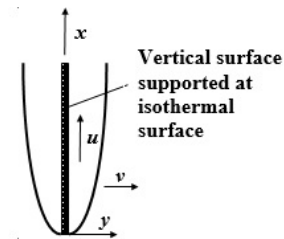


Fig. 2. Flow schematic diagram of the physical model

The governing equations of flow are given in accordance with the boundary layer assumptions which have been well adopted [48]:

$$\frac{\partial u}{\partial x} + \frac{\partial v}{\partial y} = 0, \quad (7)$$

$$u \frac{\partial u}{\partial x} + v \frac{\partial u}{\partial y} = \left( \frac{\mu}{\rho} \right) \frac{\partial^2 u}{\partial y^2} + \beta g (T - T_1), \quad (8)$$

$$u \frac{\partial T}{\partial x} + v \frac{\partial T}{\partial y} = \left( \frac{k}{\rho c_p} \right) \frac{\partial^2 T}{\partial y^2}. \quad (9)$$

We are in the case of a vertical surface, then,  $\cos \phi$  is equal to 1.

The model is of course subject to the following boundary conditions [48]:

$$\begin{aligned} \text{At } y = 0: \quad & u = v = 0, \quad T = T_w, \\ \text{For large } y: \quad & u \rightarrow 0, \quad T \rightarrow T_1. \end{aligned} \quad (10)$$

### 4.2. Similarity analysis and numerical solution procedure

We have assumed here that the velocity and temperature profiles are similar at all values of  $x$ .

Consequently, we can put:

$$\frac{u}{u_r} = \text{function} \left( \frac{y}{\delta} \right) \quad (11)$$

and

$$\frac{T - T_1}{T_w - T_1} = \text{function} \left( \frac{y}{\delta} \right), \quad (12)$$

where  $u_r$  is considered the reference velocity, and  $\delta$  simultaneously represents the thickness of the thermal boundary layer and also the local velocity.

Then, if the reference length,  $L$  is assumed to be the abscissa,  $x$ , of the leading edge of the plate, then we have

$$\delta/x = o \left[ 1/\text{Gr}_x^{0.25} \right], \quad (13)$$

with the Grashof number  $\text{Gr}_x$  expressed as a function of  $x$ , as:

$$\text{Gr}_x = \frac{\beta g (T_w - T_1) x^3}{\nu^2}. \quad (14)$$

So the local value of  $y/\delta$ , can be estimated like this

$$\eta = \frac{y}{x} \text{Gr}_x^{0.25}, \quad (15)$$

where the similarity variable here is  $\eta$ .

According to what we assumed previously, we will have

$$\frac{u}{u_r} = \text{function} (\eta), \quad (16)$$

$$\frac{T - T_1}{T_w - T_1} = \text{function}(\eta). \quad (17)$$

The characteristic velocity in the flow is given by the expression for the following reference velocity:

$$u_r = \sqrt{\beta g (T_w - T_1) x}. \quad (18)$$

So the velocity and temperature fields will take the following forms:

$$\frac{u}{\sqrt{\beta g (T_w - T_1) x}} = F'(\eta) \quad (19)$$

and

$$\frac{T - T_1}{T_w - T_1} = G(\eta). \quad (20)$$

The derived function  $F'$  represents the velocity profile while the first relation designates differentiation with respect to  $\eta$ .

Now we introduce the following dimensionless variables

$$\begin{aligned}
 U &= \frac{u}{\sqrt{\beta g (T_w - T_1) x}} = \left(\frac{ux}{v}\right) \text{Gr}_x^{-0.5}, \\
 V &= \frac{v}{\sqrt{\beta g (T_w - T_1) x}} = \left(\frac{vx}{v}\right) \text{Gr}_x^{-0.5}, \\
 \theta &= (T - T_1)/(T_w - T_1).
 \end{aligned} \tag{21}$$

After the substitution of these, the continuity equation will take the following form:

$$\frac{\partial}{\partial x} \left[ U \sqrt{\beta g (T_w - T_1) x} \right] + \frac{\partial}{\partial y} \left[ V \sqrt{\beta g (T_w - T_1) x} \right] = 0. \tag{22}$$

We will then have

$$\frac{\partial U}{\partial x} + \frac{U}{2x} + \frac{\partial V}{\partial y} = 0. \tag{23}$$

By involving the similarity variable,  $\eta$ , this equation will transform into:

$$\frac{\partial U}{\partial \eta} \frac{\partial \eta}{\partial x} + \frac{U}{2x} + \frac{\partial V}{\partial \eta} \frac{\partial \eta}{\partial y} = 0. \tag{24}$$

Using Eq. (15), defining  $\eta$ , we can derive this

$$\frac{\partial \eta}{\partial x} = -\frac{y}{4x^2} \text{Gr}_x^{0.25} = -\frac{\eta}{4x}, \tag{25}$$

$$\frac{\partial \eta}{\partial y} = \frac{\text{Gr}_x^{0.25}}{x}. \tag{26}$$

If we substitute these last two in Eq. (24), we get:

$$\frac{dF'}{d\eta} \left(-\frac{\eta}{4x}\right) + \frac{F'}{2x} + \frac{\partial V}{\partial \eta} \frac{\text{Gr}_x^{0.25}}{x} = 0. \tag{27}$$

After the simplifications and rearrangement, we arrive at

$$\frac{\partial V}{\partial \eta} = \frac{1}{2\text{Gr}_x^{0.25}} \left[ \frac{\eta}{2} \frac{dF'}{d\eta} - F' \right]. \tag{28}$$

According to Eq. (10) of the boundary conditions, we have:

$$\text{At } y = 0: \quad v = 0. \tag{29}$$

The use of boundary conditions allows us to write:

$$\text{At } \eta = 0: \quad V = 0. \tag{30}$$

Integrating Eq. (28) and applying the boundary conditions gives us:

$$V = \frac{1}{2\text{Gr}_x^{0.25}} \left[ \int \frac{\eta}{2} \frac{dF'}{d\eta} d\eta - F \right], \quad (31)$$

which tends towards:

$$V = \frac{1}{2\text{Gr}_x^{0.25}} \left[ \frac{\eta F'}{2} - \frac{F}{2} - F \right]. \quad (32)$$

From where

$$V = \frac{1}{4\text{Gr}_x^{0.25}} [\eta F' - 3F]. \quad (33)$$

The integration by parts of the first term located between brackets gives us this:

$$\int \frac{\eta}{2} \frac{dF'}{d\eta} d\eta = \int \frac{d}{d\eta} \left( \frac{\eta}{2} F' \right) d\eta - \int \frac{F'}{2} d\eta. \quad (34)$$

Introducing dimensionless variables into the momentum equation, allows us to write:

$$U \frac{\partial U}{\partial x} + \frac{U^2}{2x} + V \frac{\partial U}{\partial y} = \nu \frac{\partial^2 U}{\partial y^2} \frac{1}{\sqrt{\beta g (T_w - T_1) x}} + \frac{\theta}{x}. \quad (35)$$

That is to say

$$U \frac{\partial U}{\partial \eta} \frac{\partial \eta}{\partial x} + \frac{U^2}{2x} + V \frac{\partial U}{\partial \eta} \frac{\partial \eta}{\partial y} = \nu \frac{\partial^2 U}{\partial \eta^2} \left( \frac{\partial \eta}{\partial y} \right) \frac{1}{\sqrt{\beta g (T_w - T_1) x}} + \frac{\theta}{x}, \quad (36)$$

whence

$$F' F'' \left( -\frac{\eta}{4x} \right) + \frac{F'^2}{2x} + \frac{1}{4\text{Gr}_x^{0.25}} (\eta F' - 3F) F'' \frac{\text{Gr}_x^{0.25}}{x} = \frac{F'''}{x} + \frac{\theta}{x}. \quad (37)$$

From where

$$-\frac{\eta F' F''}{4} + \frac{F'^2}{2} + \frac{\eta F' F''}{4} - \frac{3FF''}{4} = F''' + G. \quad (38)$$

Finally, we get

$$F''' + \frac{3FF''}{4} - \frac{F'^2}{2} + G = 0. \quad (39)$$

Writing the energy equation taking into account the constant temperatures  $T_w$  and  $T_1$ , gives us:

$$U \frac{\partial \theta}{\partial x} + V \frac{\partial \theta}{\partial y} = \left( \frac{k}{\rho c_p} \right) \frac{\partial^2 \theta}{\partial y^2} \frac{1}{\sqrt{\beta g (T_w - T_1) x}}. \quad (40)$$

So we pull

$$F'G' \left( -\frac{\eta}{4x} \right) + \frac{1}{4\text{Gr}_x^{0.25}} (\eta F' - 3F) G' \frac{\text{Gr}_x^{0.25}}{x} = \frac{G''}{\text{Pr} x}. \quad (41)$$

The simplification gives

$$G'' + \frac{3}{4} \text{Pr} F G' = 0. \quad (42)$$

We finally arrive at the resolution of a system of ordinary differential equations formed simultaneously from the two equations (39) and (42) to find two functions; in this case the velocity  $F$  and the temperature  $G$ . The resolution process will of course involve the incorporation of the following boundary conditions:

$$\begin{aligned} \text{At } y = 0: \quad u = 0 &\quad \Rightarrow \quad \eta = 0: \quad F' = 0, \\ \text{At } y = 0: \quad v = 0 &\quad \Rightarrow \quad \eta = 0: \quad F = 0, \\ \text{At } y = 0: \quad T = T_w &\quad \Rightarrow \quad \eta = 0: \quad G = 1, \\ \text{For large } y: \quad u \rightarrow 0 &\quad \Rightarrow \quad \text{for large } \eta: \quad F' \rightarrow 0, \\ \text{For large } y: \quad T \rightarrow T_1 &\quad \Rightarrow \quad \text{for large } \eta: \quad G \rightarrow 0. \end{aligned} \quad (43)$$

The hypothesis of the existence of similarity solutions is fully confirmed as long as we are able to reduce the original partial differential equations describing the thermal problem to a system of ordinary differential equations. The Prandtl number,  $\text{Pr}$  is a remarkable parameter in Eq. (42) and for each value of it; a specific solution is obtained for the variation of  $F$  and  $G$  as a function of the similarity variable  $\eta$ .

Then at the wall level, we can estimate the rate of heat transfer as:

$$q_w = -k \left. \frac{\partial T}{\partial y} \right|_{y=0} = -k (T_w - T_1) \left. \frac{dG}{d\eta} \right|_{\eta=0} \frac{\text{Gr}_x^{0.25}}{x} \quad (44)$$

which give

$$\frac{\text{Nu}_x}{\text{Gr}_x^{0.25}} = -G' \Big|_{\eta=0}, \quad (45)$$

where  $\text{Nu}_x$ , is determined as; the local Nusselt number.

If we take into account equation (43) relating to boundary conditions, there are thus conditions, both at  $\eta = 0$  and at large  $\eta$ . We cannot therefore directly integrate the two equations (39) and (42). In order to find the variations of  $F$  and  $G$  with  $\eta$ , the procedure for the simultaneous solution of these equations consists in first guessing the values  $F''$  and  $G'$  at the large  $\eta$  and then proceeding to the numerical integration simultaneously of the equations (39) and (42).

In the case of boundary conditions on  $F$  and  $G$  at large  $\eta$ , the solutions obtained will generally not satisfy these. Then, we can obtain the solution by assuming other

values of  $F''$  and  $G'$  at  $\eta = 0$  and the resulting results are exploited to derive the values which provide solutions while satisfying the boundary conditions  $F'$  and  $G$  in large  $\eta$ . The simplest method is to guess the values  $F''$  and  $G'$  at  $\eta = 0$  and obtain the solution, then increase, firstly, the assumed value of  $F''$  at  $\eta = 0$  by a small amount and get the solution, and secondly, increase the assumed value of  $G'$  at  $\eta = 0$  by a small amount and get the solution. Improved guesses for the values of  $F''$  and  $G'$  at  $\eta = 0$  can then be deduced and the technique is repeated until convergence of the values of  $F''$  and  $G'$  at  $\eta = 0$  is obtained.

The method of the numerical procedure implemented for the resolution of the differential equations was adapted and programmed in FORTRAN language while using the Runge-Kutta technique of the fourth-order as a subroutine called in each step

The program as it is configured, the results from it simply give us numerical quantity of the Prandtl number up to the value of  $Pr = 30$ .

## 5. Results and discussion

Table 1 gathers all the computation results from the FORTRAN code which gives the similarity solution of two-dimensional laminar free convective boundary layer flow over a vertical flat plate with isothermal surface temperature. The results illustrated during this simulation are the function  $F(\eta)$  and its derivatives ( $F'(\eta)$  and  $F''(\eta)$ ) as well as the dimensionless temperature  $\theta(\eta)$  obtained by varying each time the value of the Prandtl number ( $Pr = 0.7, 1, 3, 10, 30$ ).

Fig. 3 illustrates some typical profiles of the velocity field which were obtained using the numerical procedure implemented in this program for various Prandtl numbers  $Pr$ . The flow spaced from the vertical surface is stationary, as long as an extensive medium is considered here. Because of the no-slip condition, the flow next to the surface is stationary in nature. As this figure illustrates, on each side, the flow is distinguished in a layer adjacent to the surface with, of course, zero vertical velocity. The temperature changes from  $T_w$  to  $T_1$  which implies that the maximum vertical speed is generated at a certain distance from the surface at which its exact value is determined experimentally. According to this figure, we found that the maximum dimensionless velocity decreases, and the increase in  $Pr$  also causes the velocity gradient at the surface to decrease showing the effect of a larger viscous force. As long as the Prandtl number decreases to low values, we see that the thickness of the velocity boundary layer increases identically.

Fig. 4 clearly shows the evolution of the dimensionless temperature as a function of the similarity variable by playing on the variation of the Prandtl number values. One can notice from this figure that the increase in the value of the Prandtl number tends to a decrease in the thickness of the thermal boundary layer, and to an increase in the absolute value of the temperature gradient at the surface. Indeed, according to the physical significance of the Prandtl number, this result is pertinently expected, since this number compares the speed of thermal phenomena and

Table 1. Computational results outputs of the numerical simulation

a)  $Pr = 0.7$ 

$\eta$	$F$	$dF/d\eta$	$d^2F/d\eta^2$	$G = \theta$
0.000000	0.000000	0.000000	0.958222	1.000000
0.030000	0.000427	0.028298	0.928382	0.989401
0.060000	0.001689	0.055706	0.898867	0.978802
0.120000	0.006614	0.107890	0.840832	0.957607
0.180000	0.014567	0.156633	0.784168	0.936416
0.300000	0.038744	0.244133	0.675141	0.894071
0.600000	0.138533	0.408852	0.429688	0.788871
0.900000	0.277311	0.506161	0.226292	0.685990
0.990000	0.323710	0.524137	0.173836	0.655887
1.005000	0.331591	0.526682	0.165481	0.650912
2.010000	0.870945	0.492243	-0.16265	0.359019
3.000000	1.267433	0.305737	-0.18471	0.173699
4.005000	1.491734	0.152027	-0.11820	0.075239
5.010000	1.595554	0.064257	-0.060586	0.029944
6.000000	1.635738	0.022342	-0.02757	0.010510
7.005000	1.647628	0.004109	-0.01077	0.002109
7.485000	1.648548	0.000084	-0.00627	0.000046

b)  $Pr = 1$ 

$\eta$	$F$	$dF/d\eta$	$d^2F/d\eta^2$	$G = \theta$
0.000000	0.000000	0.000000	0.907472	1.000000
0.030000	0.000404	0.026776	0.877654	0.987974
0.060000	0.001598	0.052663	0.848201	0.975948
0.120000	0.006249	0.101814	0.790418	0.951898
0.180000	0.013747	0.147544	0.734166	0.927855
0.300000	0.036476	0.229114	0.626424	0.879824
0.600000	0.129639	0.379981	0.386588	0.760755
0.900000	0.257933	0.465553	0.191516	0.645177
0.990000	0.300540	0.480527	0.141927	0.611637
1.005000	0.307763	0.482597	0.134062	0.606110
2.010000	0.792700	0.433639	-0.16120	0.294568
3.000000	1.135384	0.258312	-0.16703	0.120571
4.005000	1.321415	0.123241	-0.10060	0.043239
5.010000	1.404281	0.050348	-0.04884	0.014265
6.000000	1.435495	0.017225	-0.02131	0.004229
7.005000	1.444688	0.003224	-0.008315	0.000735
7.485000	1.445416	0.000068	-0.00506	0.00001

Table 1 [cont.]

c) Pr = 3

$\eta$	$F$	$dF/d\eta$	$d^2F/d\eta^2$	$G = \theta$
0.000000	0.000000	0.000000	0.750420	1.000000
0.030000	0.000333	0.022065	0.720680	0.982710
0.060000	0.001315	0.043246	0.691462	0.965421
0.120000	0.005120	0.083018	0.634610	0.930850
0.180000	0.011210	0.119442	0.579891	0.896303
0.300000	0.029466	0.182766	0.476959	0.827406
0.600000	0.102271	0.291671	0.258358	0.658609
0.900000	0.198743	0.343303	0.094841	0.501223
0.990000	0.229971	0.350059	0.056050	0.457521
1.005000	0.235228	0.350855	0.050023	0.450426
2.010000	0.566211	0.278395	-0.13194	0.120970
3.000000	0.778396	0.155236	-0.10472	0.021783
4.005000	0.890041	0.074910	-0.05754	0.002970
5.010000	0.941896	0.033106	-0.02865	0.000356
6.000000	0.963440	0.012810	-0.01403	0.000040
7.005000	0.970677	0.002801	-0.00676	0.000003
7.485000	0.971327	0.000064	-0.00476	0.000000

d) Pr = 10

$\eta$	$F$	$dF/d\eta$	$d^2F/d\eta^2$	$G = \theta$
0.000000	0.000000	0.000000	0.592177	1.000000
0.030000	0.000262	0.017319	0.562549	0.975221
0.060000	0.001030	0.033760	0.533667	0.950444
0.120000	0.003983	0.064100	0.478148	0.900915
0.180000	0.008658	0.091198	0.425636	0.851477
0.300000	0.022428	0.136395	0.329660	0.753323
0.600000	0.075088	0.205277	0.141710	0.519991
0.900000	0.141017	0.228272	0.021986	0.323021
0.990000	0.161615	0.229110	-0.00257	0.273921
1.005000	0.165052	0.229044	-0.00622	0.266229
2.010000	0.368975	0.166113	-0.07814	0.021041
3.000000	0.498698	0.100083	-0.05403	0.000639
4.005000	0.575785	0.056733	-0.03366	0.000010
5.010000	0.618238	0.029912	-0.02072	0.000000
6.000000	0.639145	0.013626	-0.01280	0.000000
7.005000	0.647309	0.003446	-0.00785	0.000000
7.485000	0.648125	0.000084	-0.00622	0.000000

Table 1 [cont.]

e) Pr = 30

$\eta$	$F$	$dF/d\eta$	$d^2F/d\eta^2$	$G = \theta$
0.000000	0.000000	0.000000	0.467453	1.000000
0.030000	0.000206	0.013579	0.437958	0.966347
0.060000	0.000806	0.026288	0.409474	0.932700
0.120000	0.003087	0.049218	0.355543	0.865483
0.180000	0.006650	0.069034	0.305660	0.798556
0.300000	0.016915	0.100291	0.217954	0.666926
0.600000	0.054177	0.140501	0.065138	0.372451
0.900000	0.097886	0.147147	-0.01034	0.167114
0.990000	0.111070	0.145647	-0.02236	0.125544
1.005000	0.113252	0.145299	-0.02400	0.119452
2.010000	0.239589	0.104334	-0.04065	0.001182
3.000000	0.324821	0.069656	-0.02977	0.000001
4.005000	0.381309	0.044159	-0.02139	-0.00000
5.010000	0.415992	0.025880	-0.01531	-0.00000
6.000000	0.434872	0.012973	-0.01100	-0.00000
7.005000	0.442927	0.003581	-0.00786	-0.00000
7.485000	0.443786	0.000091	-0.00670	-0.00000

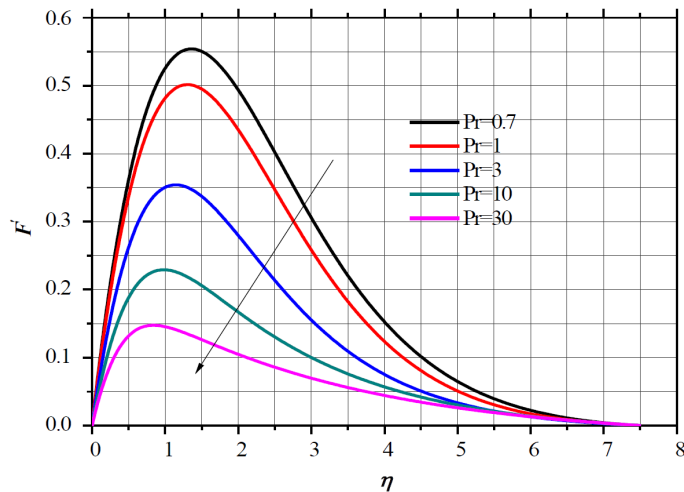


Fig. 3. Dimensionless velocity profiles for different values of the Prandtl number

hydrodynamic phenomena in a fluid. In other words, it indicates the comparison between momentum and thermal diffusion. The magnification of the Prandtl number values indicates the presence of increasing viscous effects. Due to the nature

of the coupling of the velocity and temperature fields in natural convection, the velocity boundary layer cannot be thinner than the thermal boundary layer. It is also exciting to note that the results show the coupling between the velocity and temperature fields, as asserted by the existence of flow wherever a temperature difference exists, such as low Pr profiles.

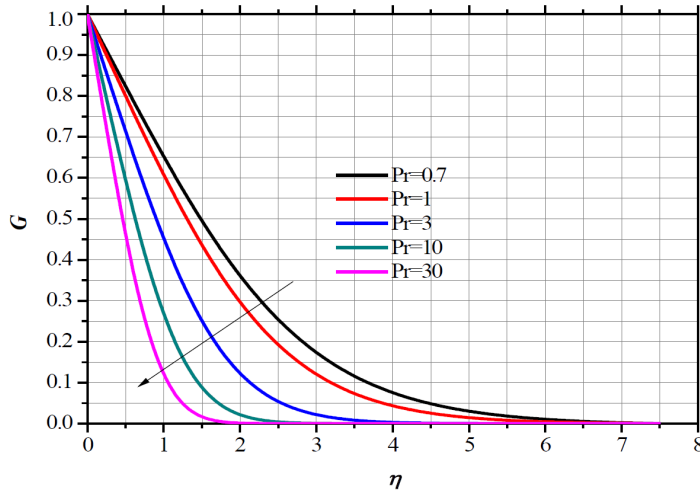


Fig. 4. Dimensionless temperature profiles for different values of the Prandtl number

In Fig. 5, we have plotted the dimensionless temperature profile  $\theta$  in three-dimensions 3D according to the  $x$  coordinate as similarity variable  $\eta$  and the  $y$

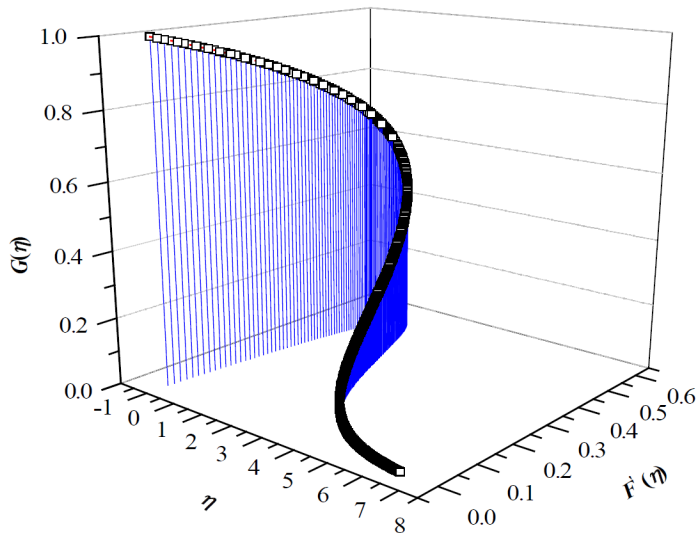


Fig. 5. 3D plot of dimensionless temperature contours as a function of similarity variable and the velocity profile

coordinate as velocity. Commonly, at the surface of the plate, the fluid has a maximum temperature, which decreases exponentially to zero far from the plate satisfying the boundary condition.

The effect of various values of the Prandtl number on function profiles  $F(\eta)$  in the boundary layer is depicted in Fig. 6. It is observed in Fig. 6, that the variation of the function starts from a zero value at the plate surface and increases to the free stream value far away from the plate surface satisfying the far-field boundary condition.

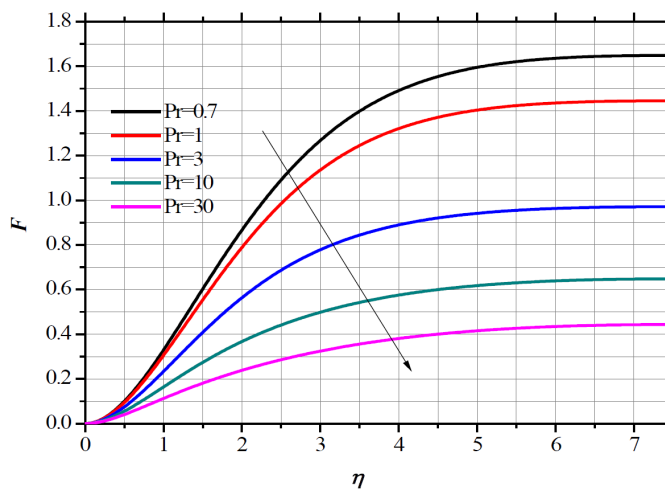


Fig. 6. Plot of the function  $F$  versus  $\eta$  in free laminar convective flow over the vertical plate for various values of the Prandtl number

Increasing  $Pr$  means that the viscous force increases and thermal diffusivity reduces, which causes a reduction in the velocity and temperature, as expected. It is also noticed that the time is taken to reach steady-state flow increases and thermal boundary layer thickness reduces with increasing  $Pr$ . Further, it is clearly seen from Fig. 6 that the momentum boundary layer thickness increases with the increase of  $Pr$  from unity.

As shown in Fig. 7, we plotted the evolution of the three functions ( $F$ ,  $F'$  and  $F''$ ) obtained using computer code for the same value of the Prandtl number  $Pr = 0.7$ . It is noted that the curves of the last two functions follow the same behavior of the velocity and temperature fields.

Fig. 8 depicts the variation of the function  $d^2F/d\eta^2$  with respect to  $\eta$  for different values of the Prandtl number. Generally, the fluid velocity increases gradually away from the plate, attains its peak value within the boundary layer, and then decreases to the free stream zero value satisfying the boundary conditions. The fluid temperature is highest near the plate surface and decreases exponentially to zero value far away from the plate. At a certain distance from the plate boundary, a very thin layer is formed which is streamlined in shape. This may imply a steep gradient

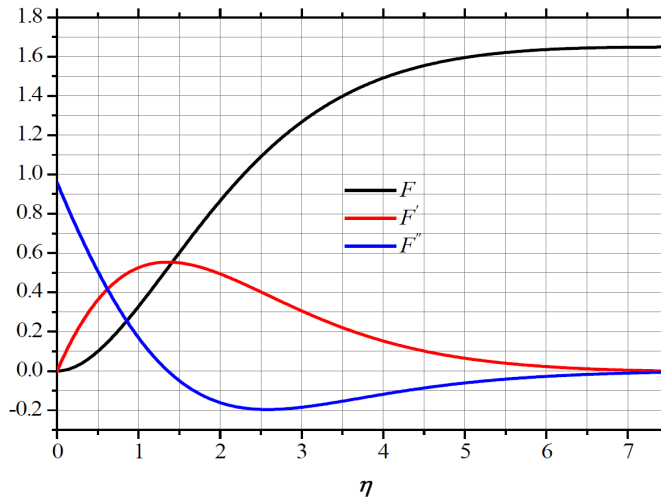


Fig. 7. The graphical representations of  $F$  and its derivatives at  $Pr = 0.7$

of shearing stress. The variation in the layout or the inflection points noticed with the shape of the curves are due to the presence of the buoyant forces acting on the fluid as it flows over the surface.

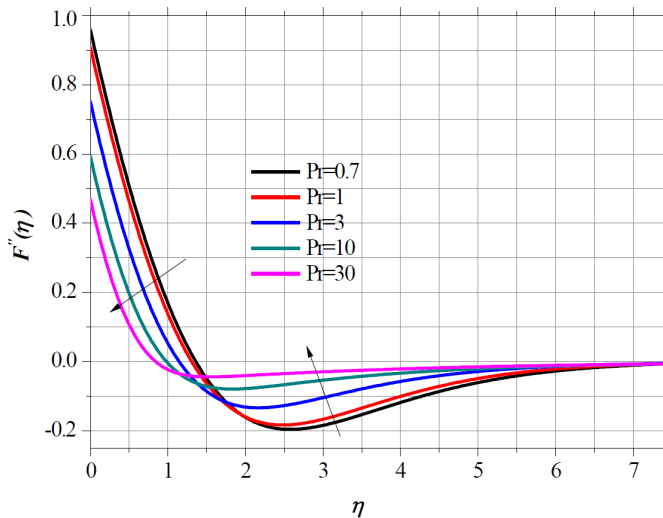


Fig. 8. Variation of the function  $d^2F/d\eta^2$  with respect to  $\eta$  for different values of Prandtl number

In Fig. 9, we have plotted the velocity profiles  $dF/d\eta$  according to the axial variation of the function  $F(\eta)$ . We can see that the shapes of the speed curves are well organized and almost elliptical in shape. We also distinguish that the increase in the Prandtl numbers  $Pr$  leads to the decrease of  $F'(\eta)$  for the boundary conditions on the plate.

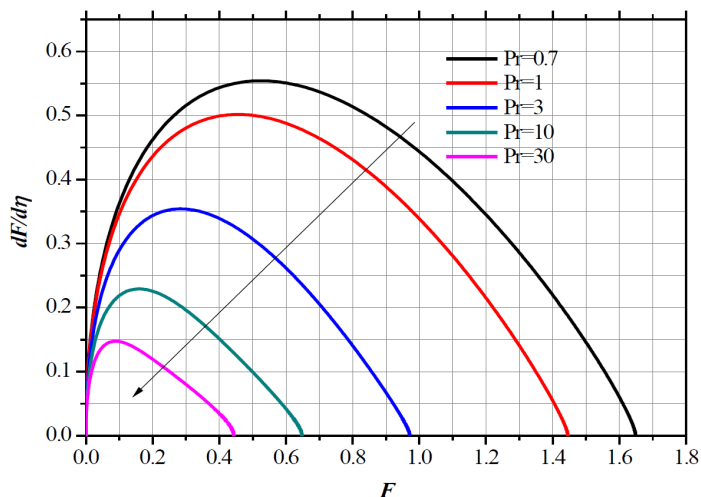


Fig. 9. Variation of the velocity function  $dF/d\eta$  with  $F$  for different values of  $Pr$

Fig. 10 obviously illustrates the behavior of the temperature profiles in the boundary layer as a function of the variation of the flow velocity. The thickness of the boundary layer increases in the flow direction. On the surface, the fluid temperature is equal to the plate temperature and gradually decreases to the temperature of the surrounding fluid at a distance sufficiently far from the surface.

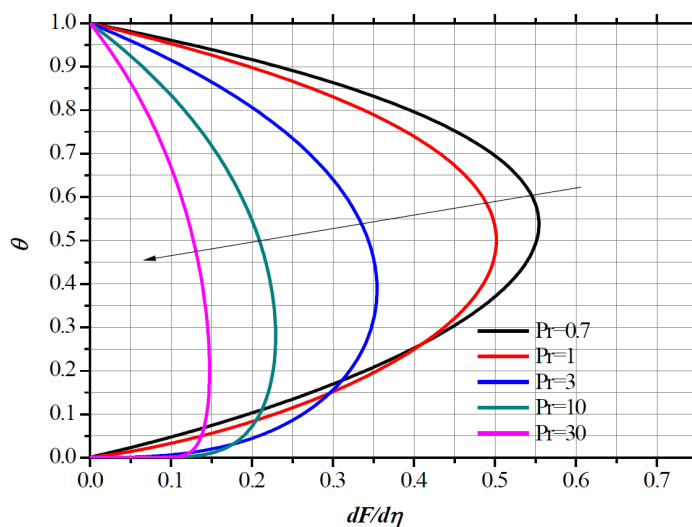


Fig. 10. Temperature profiles versus velocity for various values of  $Pr$

Table 2 shows the values of function  $A$  for different values of the Prandtl number.

Table 2. Values of  $A$  for different values of the Prandtl number

Pr	$A = -G' _{\eta=0}$	$-G' _{\eta=0}/\text{Pr}^{0.25}$
0.01	0.0570	0.1802
0.03	0.0962	0.2312
0.09	0.1549	0.28287
0.72	0.3568	0.3873
1	0.4010	0.4010
2	0.5066	0.4260
5	0.6746	0.4511
10	0.8259	0.4644
100	1.549	0.4898
1000	2.807	0.4992

The values of  $G$  were estimated approximately according to the following equation:

$$\frac{\text{Nu}_x}{\text{Gr}_x^{0.25}} = -G'|_{\eta=0} = \left[ \frac{0.316 \text{Pr}^{5/4}}{2.44 + 4.88 \text{Pr}^{1/2} + 4.95 \text{Pr}} \right]^{1/4}. \quad (46)$$

For a plate of length  $L$ , the average heat transfer rate is obtained by:

$$\bar{q}_w = \frac{1}{L} \int_0^L q_w dx. \quad (47)$$

Using the Eq. (45), we get

$$\bar{q}_w = \frac{1}{L} \int_0^L \left[ -k (T_w - T_1) G'|_{\eta=0} \frac{\text{Gr}_x^{0.25}}{x} dx \right], \quad (48)$$

$$\frac{\bar{q}_w L}{(T_w - T_1) k} = G'|_{\eta=0} \frac{4}{3} \text{Gr}_L^{0.25}, \quad (49)$$

where  $\text{Gr}_L$  is the Grashof number as a function of plate length,  $L$ . The average Nusselt number for the entire plate,  $\text{Nu}_L$  can be expressed by the following formula:

$$\frac{\text{Nu}_L}{\text{Gr}_L^{0.25}} = \frac{4}{3} G'|_{\eta=0}. \quad (50)$$

## 6. Validation of the numerical approach

In order to validate our numerical model, we carried out deep bibliographic research which was related to the subject of the contribution, and we came across the literature on the numerical results of a simulation which was conducted by

Ostrach [47]. Table 3 groups separately the numerical results of our model and those obtained by the said authors. We were able to demonstrate clearly how our numerical results are in excellent agreement with previous results, those that exist in the literature.

Table 3. Comparison of values of  $\theta$  obtained by the present similarity method with previously published results

$\eta$	$\theta(\eta)$ present work)	$\theta(\eta)$ similarity analysis by Ostrach [47]
0	1.0000	1.0000
0.2	0.8858	0.8867
0.4	0.7725	0.7742
0.9	0.5102	0.5109
1.5	0.2656	0.2684
4.4	0.0037	0.0038
5.5	0.00059	0.0006
6.25	0.0000	0.0000

We have validated our results by comparing the dimensionless temperature profile ( $\theta$ ) for  $Pr = 1$  with the numerical results obtained by Ostrach [47] in Fig. 11. It is also noted that the two graphs of the dimensionless temperature ( $\theta$ ) are perfectly confused; consequently, we can say here that there is an excellent concordance between the results of the present investigation and those of the previous works.

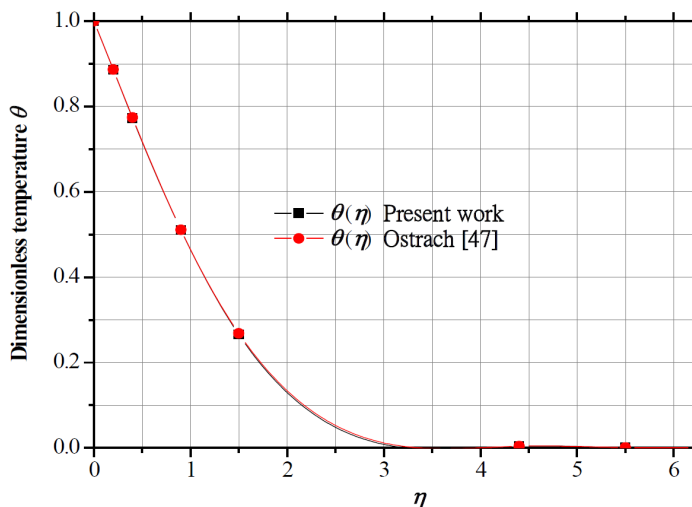


Fig. 11. The comparison of numerical results obtained in the present work and Ostrach's results for  $\theta(\eta)$

## 7. Conclusion

In this research work, a problem of natural convection heat transfer from an isothermal vertical flat heated plate has been investigated numerically by the technique of similarity solutions. The analysis was carried out with an assumed stable and laminar two-dimensional flow and the properties of the fluid (except the density) were taken as constants. Other helping assumptions have been considered here such as; the neglect of viscous dissipation effects and, no heat source was considered in the flow. Therefore, the problem was considerably simplified, although the complications due to the coupled partial differential equations remained. The computational strategy was focused on exploiting an important method for solving boundary layer flow over a heated vertical surface, it was the similarity variable method. The non-linear governing equations describing the physical model have been reduced to a system of ordinary differential equations (ODE) through well-defined similarity transformations. The obtained system of nonlinear ordinary differential equations satisfying all the boundary conditions was solved numerically and simultaneously using the Runge-Kutta of order 4. The approach of the investigation allowed us to program in the FORTRAN language, all these equations to find the numerical solution to the thermal problem for Prandtl number values up to about 30. The initial guessed values must be altered to obtain solutions at higher values of the Prandtl number.

To illustrate the effectiveness of the proposed procedure, several important thermal results have also been tabulated and presented in graphical forms and then discussed in depth -These included: dimensionless velocity and temperature profiles in the natural convective boundary layer on a vertical plate, the variation of the function  $F$  and its derivatives, the effect of the Prandtl number, the rate heat transfer and the local Nusselt number expressions with Grashof number, and the mean heat transfer for the entire plate.

From the thermal analysis of the numerical results, we were able to draw the following conclusions

- The increase in values of the Prandtl number  $Pr$  leads to a decrease in the thickness of the thermal boundary layer.
- The increase in values of the Prandtl number  $Pr$  leads to an increase in the absolute value of the temperature gradient at the surface and, this was expected given the nature and physical meaning of the Prandtl number, which gives the comparison between momentum and thermal diffusion.
- The increase in the values of the Prandtl number  $Pr$  indicates the increase in the viscous effects.
- With increasing  $Pr$ , the velocity gradient at the surface and the maximum dimensionless velocity are also decreased due to the existence of the effect of larger viscous forces.
- The location of the dimensionless temperature maximum value has a tendency to shift right to higher  $\eta$  as  $Pr$  is decreased.

- The thickness of the velocity boundary layer also has a tendency to increase when  $Pr$  is decreased to lower values.
- The numerical model treated was perfectly validated and it was found in good agreement with the investigations in the old research works.
- It is also noteworthy that the numerical results of this simulation show the coupling between the velocity and temperature fields, as evidenced by the regularity of flow wherever there is a temperature difference, such as the profiles with low values of Prandtl number  $Pr$ .

From the numerical results obtained, we can confirm that some properties related to the Prandtl number are verified. The effect of the Prandtl number,  $Pr$ , on the thickness of the thermal boundary layer has been effectively tested. The buoyancy force and the Prandtl number significantly increase the surface shear stress and the surface heat transfer. Also for small values of the Prandtl number and for streamwise distances, the surface shear stress changes very significantly. The influence of  $Pr$  on the local skin-friction and the local Nusselt number increases along the surface from a certain distance from the plate. At this stage, we do not have any comparison with experimental data due to the absence of such data. Thus, this work bears fruit presenting a fundamental aspect which deals with the problem of natural convection in a vertical plate and heat transfer correlations which can be used for severely practical industrial applications.

It is hoped that the current results will be useful for understanding more complex problems dealing with mixed convection and will stimulate interest in experimental work.

## References

- [1] Md J. Uddin, W.A. Khan, and A.I. Md Ismail. Similarity solution of double diffusive free convective flow over a moving vertical flat plate with convective boundary condition. *Ain Shams Engineering Journal*, 6(3):1105–1112, 2015. doi: [10.1016/j.asej.2015.01.008](https://doi.org/10.1016/j.asej.2015.01.008).
- [2] J.A. Esfahani and B. Bagherian. Similarity solution for unsteady free convection from a vertical plate at constant temperature to power law fluids. *Journal of Heat Transfer*, 134(10):1–7, 2012. doi: [10.1115/1.4005750](https://doi.org/10.1115/1.4005750).
- [3] Y.Z. Boutros, M.B. Abd-el-Malek, and N.A. Badran. Group theoretic approach for solving time-independent free-convective boundary layer flow on a nonisothermal vertical flat plate. *Archiwum Mechaniki Stosowanej*, 42(3):377–395, 1990.
- [4] M. Modather, A.M. Rashad, and A.J. Chamkha. An analytical study of MHD heat and mass transfer oscillatory flow of a micropolar fluid over a vertical permeable plate in a porous medium. *Turkish Journal of Engineering and Environmental Sciences*, 33(4):245–257, 2009.
- [5] M.V. Krishna and A.J. Chamkha. Hall and ion slip effects on MHD rotating flow of elasticoviscous fluid through porous medium. *International Communications in Heat and Mass Transfer*, 113:104494, 2020. doi: [10.1016/j.icheatmasstransfer.2020.104494](https://doi.org/10.1016/j.icheatmasstransfer.2020.104494).
- [6] M.V. Krishna and A.J. Chamkha. Hall and ion slip effects on MHD rotating boundary layer flow of nanofluid past an infinite vertical plate embedded in a porous medium. *Results in Physics*, 15:102652, 2019. doi: [10.1016/j.rinp.2019.102652](https://doi.org/10.1016/j.rinp.2019.102652).

- [7] M.V. Krishna, N.A. Ahamad, and A.J. Chamkha. Hall and ion slip effects on unsteady MHD free convective rotating flow through a saturated porous medium over an exponential accelerated plate. *Alexandria Engineering Journal*, 59(2):565–577, 2020. doi: [10.1016/j.aej.2020.01.043](https://doi.org/10.1016/j.aej.2020.01.043).
- [8] A.J. Chamkha. Non-Darcy fully developed mixed convection in a porous medium channel with heat generation/absorption and hydromagnetic effects. *Numerical Heat Transfer, Part A: Applications*, 32(6):653–675, 1997. doi: [10.1080/10407789708913911](https://doi.org/10.1080/10407789708913911).
- [9] A.J. Chamkha. Thermal radiation and buoyancy effects on hydromagnetic flow over an accelerating permeable surface with heat source or sink. *International Journal of Engineering Science*, 38(15):1699–1712, 2000. doi: [10.1016/S0020-7225\(99\)00134-2](https://doi.org/10.1016/S0020-7225(99)00134-2).
- [10] G. Rasool, T. Zhang, A.J. Chamkha, A. Shafiq, I. Tlili, and G. Shahzadi. Entropy generation and consequences of binary chemical reaction on MHD Darcy–Forchheimer Williamson nanofluid flow over non-linearly stretching surface. *Entropy*, 22(18):18, 2020. doi: [10.3390/e22010018](https://doi.org/10.3390/e22010018).
- [11] A.J. Chamkha, C. Issa, and K. Khanafer. Natural convection from an inclined plate embedded in a variable porosity porous medium due to solar radiation. *International Journal of Thermal Sciences*, 41(1):73–81, 2002. doi: [10.1016/S1290-0729\(01\)01305-9](https://doi.org/10.1016/S1290-0729(01)01305-9).
- [12] A.J. Chamkha and A. Ben-Nakhi. MHD mixed convection-radiation interaction along a permeable surface immersed in a porous medium in the presence of Soret and Dufour’s effects. *Heat and Mass Transfer*, 44:845, 2008. doi: [10.1007/s00231-007-0296-x](https://doi.org/10.1007/s00231-007-0296-x).
- [13] A.J. Chamkha. Hydromagnetic natural convection from an isothermal inclined surface adjacent to a thermally stratified porous medium. *International Journal of Engineering Science*, 35(10/11):975–986, 1997. doi: [10.1016/S0020-7225\(96\)00122-X](https://doi.org/10.1016/S0020-7225(96)00122-X).
- [14] A. Wakif, A.J. Chamkha, I.L. Animasaun, M. Zaydan, H. Waqas, and R. Sehaqui. Novel physical insights into the thermodynamic irreversibilities within dissipative EMHD fluid flows past over a moving horizontal Riga plate in the coexistence of wall suction and Joule heating effects: A comprehensive numerical investigation. *Arabian Journal for Science and Engineering*, 45:9423–9438, 2020. doi: [10.1007/s13369-020-04757-3](https://doi.org/10.1007/s13369-020-04757-3).
- [15] N.A. Ahammad, I.A. Badruddin, S.Z. Kamangar, H.M.T. Khaleed, C.A. Saleel, and T.M.I. Mahlia. Heat Transfer and entropy in a vertical porous plate subjected to suction velocity and MHD. *Entropy*, 23(8):1069, 2021. doi: [10.3390/e23081069](https://doi.org/10.3390/e23081069).
- [16] M.V. Krishna, N.A. Ahamad, and A.J. Chamkha. Numerical investigation on unsteady MHD convective rotating flow past an infinite vertical moving porous surface. *Ain Shams Engineering Journal*, 12(2): 2099–2109, 2021. doi: [10.1016/j.asej.2020.10.013](https://doi.org/10.1016/j.asej.2020.10.013).
- [17] P. Kandaswamy, A.K.A. Hakeem, and S. Saravanan. Internal natural convection driven by an orthogonal pair of differentially heated plates. *Computers & Fluids*, 111:179–186, 2015. doi: [10.1016/j.compfluid.2015.01.015](https://doi.org/10.1016/j.compfluid.2015.01.015).
- [18] S.E. Ahmed, H.F. Oztop, and K. Al-Salem. Natural convection coupled with radiation heat transfer in an inclined porous cavity with corner heater. *Computers & Fluids*, 102:74–84, 2014. doi: [10.1016/j.compfluid.2014.06.024](https://doi.org/10.1016/j.compfluid.2014.06.024).
- [19] S. Siddiqa, M.A. Hossain, and R.S.R. Gorla. Natural convection flow of viscous fluid over triangular wavy horizontal surface. *Computers & Fluids*, 106:130–134, 2015. doi: [10.1016/j.compfluid.2014.10.001](https://doi.org/10.1016/j.compfluid.2014.10.001).
- [20] L. Zhou, S.W. Armfield, N. Williamson, M.P. Kirkpatrick, and W. Lin. Natural convection in a cavity with time-dependent flux boundary. *International Journal of Heat and Fluid Flow*, 92:108887, 2021. doi: [10.1016/j.ijheatfluidflow.2021.108887](https://doi.org/10.1016/j.ijheatfluidflow.2021.108887).
- [21] K.M. Talluru, H.F. Pan, J.C. Patterson, and K.A. Chauhan. Convection velocity of temperature fluctuations in a natural convection boundary layer. *International Journal of Heat and Fluid Flow*, 84:108590, 2020. doi: [10.1016/j.ijheatfluidflow.2020.108590](https://doi.org/10.1016/j.ijheatfluidflow.2020.108590).

- [22] M. Chakkingal, S. Kenjereš, I. Ataei-Dadavi, M.J. Tummers, and C.R. Kleijn. Numerical analysis of natural convection with conjugate heat transfer in coarse-grained porous media. *International Journal of Heat and Fluid Flow*, 77:48–60, 2019. doi: [10.1016/j.ijheatfluidflow.2019.03.008](https://doi.org/10.1016/j.ijheatfluidflow.2019.03.008).
- [23] N. Mahir and Z. Altaç. Numerical investigation of flow and combined natural-forced convection from an isothermal square cylinder in cross flow. *International Journal of Heat and Fluid Flow*, 75:103–121, 2019. doi: [10.1016/j.ijheatfluidflow.2018.11.013](https://doi.org/10.1016/j.ijheatfluidflow.2018.11.013).
- [24] M.A. Ezan and M. Kalfa. Numerical investigation of transient natural convection heat transfer of freezing water in a square cavity. *International Journal of Heat and Fluid Flow*, 61(Part B):438–448, 2016. doi: [10.1016/j.ijheatfluidflow.2016.06.004](https://doi.org/10.1016/j.ijheatfluidflow.2016.06.004).
- [25] A. Ouahouah, N. Labsi, X. Chesneau, and Y.K. Benkahla. Natural convection within a non-uniformly heated cavity partly filled with a shear-thinning nanofluid and partly with air. *Journal of Non-Newtonian Fluid Mechanics*, 289:104490, 2021. doi: [10.1016/j.jnnfm.2021.104490](https://doi.org/10.1016/j.jnnfm.2021.104490).
- [26] M.H. Matin, I. Pop, and S. Khanchezar. Natural convection of power-law fluid between two-square eccentric duct annuli. *Journal of Non-Newtonian Fluid Mechanics*, 197:11–23, 2013. doi: [10.1016/j.jnnfm.2013.02.002](https://doi.org/10.1016/j.jnnfm.2013.02.002).
- [27] M.T. Nguyen, A.M. Aly, and S.W. Lee. A numerical study on unsteady natural/ mixed convection in a cavity with fixed and moving rigid bodies using the ISPH method. *International Journal of Numerical Methods for Heat & Fluid Flow*, 28(3):684–703, 2018. doi: [10.1108/HFF-02-2017-0058](https://doi.org/10.1108/HFF-02-2017-0058).
- [28] Y. Guo, R. Bennacer, S. Shen, D.E. Ameziani, and M. Bouzidi. Simulation of mixed convection in slender rectangular cavity with lattice Boltzmann method. *International Journal of Numerical Methods for Heat & Fluid Flow*, 20(1):130–148, 2010. doi: [10.1108/09615531011008163](https://doi.org/10.1108/09615531011008163).
- [29] N.B. Balam and A. Gupta. A fourth-order accurate finite difference method to evaluate the true transient behaviour of natural convection flow in enclosures. *International Journal of Numerical Methods for Heat & Fluid Flow*, 30(3):1233–1290, 2020. doi: [10.1108/HFF-06-2019-0519](https://doi.org/10.1108/HFF-06-2019-0519).
- [30] L. Lukose and T. Basak. Numerical heat flow visualization analysis on enhanced thermal processing for various shapes of containers during thermal convection. *International Journal of Numerical Methods for Heat & Fluid Flow*, 30(7):3535–3583, 2020. doi: [10.1108/HFF-05-2019-0376](https://doi.org/10.1108/HFF-05-2019-0376).
- [31] P. Pichandi and S. Anbalagan. Natural convection heat transfer and fluid flow analysis in a 2D square enclosure with sinusoidal wave and different convection mechanism. *International Journal of Numerical Methods for Heat & Fluid Flow*, 28(9):2158–2188, 2018. doi: [10.1108/HFF-12-2017-0522](https://doi.org/10.1108/HFF-12-2017-0522).
- [32] M. Salari, M.M. Rashidi, E.H. Malekshah, and M.H. Malekshah. Numerical analysis of turbulent/transitional natural convection in trapezoidal enclosures. *International Journal of Numerical Methods for Heat & Fluid Flow*, 27(12):2902–2923, 2017. doi: [10.1108/HFF-03-2017-0097](https://doi.org/10.1108/HFF-03-2017-0097).
- [33] A. Salama, M. El Amin, and S. Sun. Numerical investigation of natural convection in two enclosures separated by anisotropic solid wall. *International Journal of Numerical Methods for Heat & Fluid Flow*, 24(8):1928–1953, 2014. doi: [10.1108/HFF-09-2013-0268](https://doi.org/10.1108/HFF-09-2013-0268).
- [34] N. Kim and J.N. Reddy. Least-squares finite element analysis of three-dimensional natural convection of generalized Newtonian fluids. *International Journal for Numerical Methods in Fluids*, 93(4):1292–1307, 2021. doi: [10.1002/fld.4929](https://doi.org/10.1002/fld.4929).
- [35] J. Zhang and F. Lin. An efficient Legendre-Galerkin spectral method for the natural convection in two-dimensional cavities. *International Journal for Numerical Methods in Fluids*, 90(12):651–659, 2019. doi: [10.1002/fld.4742](https://doi.org/10.1002/fld.4742).
- [36] J.C.F. Wong and P. Yuan. A FE-based algorithm for the inverse natural convection problem. *International Journal for Numerical Methods in Fluids*, 68(1):48–82, 2012. doi: [10.1002/fld.2494](https://doi.org/10.1002/fld.2494).

- [37] H.S. Panda and S.G. Moulic. An analytical solution for natural convective gas micro flow in a tall vertical enclosure. *Proceedings of the Institution of Mechanical Engineers, Part C: Journal of Mechanical Engineering Science*, 225(1):145–154, 2011. doi: [10.1243/09544062JMES1768](https://doi.org/10.1243/09544062JMES1768).
- [38] M. Saleem, S. Asghar, and M.A. Hossain. Natural convection flow in an open rectangular cavity with cold sidewalls and constant volumetric heat source. *Proceedings of the Institution of Mechanical Engineers, Part C: Journal of Mechanical Engineering Science*, 225(5):1191–1201, 2011. doi: [10.1177/09544062JMES2648](https://doi.org/10.1177/09544062JMES2648).
- [39] A. Koca, H.F. Oztop, and Y. Varol. Natural convection analysis for both protruding and flush-mounted heaters located in triangular enclosure. *Proceedings of the Institution of Mechanical Engineers, Part C: Journal of Mechanical Engineering Science*, 222(7):1203–1214, 2008. doi: [10.1243/09544062JMES886](https://doi.org/10.1243/09544062JMES886).
- [40] M.K. Mansour. Effect of natural convection on conjugate heat transfer characteristics in liquid mini channel during phase change material melting. *Proceedings of the Institution of Mechanical Engineers, Part C: Journal of Mechanical Engineering Science*, 228(3):491–513, 2014. doi: [10.1177/0954406213486590](https://doi.org/10.1177/0954406213486590).
- [41] E.F. Kent. Numerical analysis of laminar natural convection in isosceles triangular enclosures. *Proceedings of the Institution of Mechanical Engineers, Part C: Journal of Mechanical Engineering Science*, 223(5):1157–1169, 2009. doi: [10.1243/09544062JMES1122](https://doi.org/10.1243/09544062JMES1122).
- [42] A. Belhocine and W.Z. Wan Omar. An analytical method for solving exact solutions of the convective heat transfer in fully developed laminar flow through a circular tube. *Heat Transfer Asian Research*, 46(8):1342–1353, 2017. doi: [10.1002/htj.21277](https://doi.org/10.1002/htj.21277).
- [43] A. Belhocine and W. Z. Wan Omar. Numerical study of heat convective mass transfer in a fully developed laminar flow with constant wall temperature. *Case Studies in Thermal Engineering*, 6:116–127, 2015. doi: [10.1016/j.csite.2015.08.003](https://doi.org/10.1016/j.csite.2015.08.003).
- [44] A. Belhocine and O.I. Abdullah. Numerical simulation of thermally developing turbulent flow through a cylindrical tube. *International Journal of Advanced Manufacturing Technology*, 102(5-8):2001–2012, 2019. doi: [10.1007/s00170-019-03315-y](https://doi.org/10.1007/s00170-019-03315-y).
- [45] A. Belhocine and W.Z. Wan Omar. Analytical solution and numerical simulation of the generalized Levêque equation to predict the thermal boundary layer. *Mathematics and Computers in Simulation*, 180:43–60, 2021. doi: [10.1016/j.matcom.2020.08.007](https://doi.org/10.1016/j.matcom.2020.08.007).
- [46] A. Belhocine, N. Stojanovic, and O.I. Abdullah. Numerical simulation of laminar boundary layer flow over a horizontal flat plate in external incompressible viscous fluid. *European Journal of Computational Mechanics*, 30(4-6):337–386, 2021. doi: [10.13052/ejcm2642-2085.30463](https://doi.org/10.13052/ejcm2642-2085.30463).
- [47] S. Ostrach. An analysis of laminar free convection flow and heat transfer about a flat plate parallel to the direction of the generating body force. National Advisory Committee for Aeronautics, Report 1111, 1953.
- [48] T.L. Bergman, A.S. Lavine, F.P. Incropera, and D.P. Dewitt. *Fundamentals of Heat and Mass Transfer*, 7th ed., John Wiley & Sons, New York, 2011.